INL/CON-15-35979
PREPRINT

SCALE ANALYSIS AND EXPERIMENTAL RESULTS OF A SOLID/LIQUID PHASE-CHANGE THERMAL ENERGY STORAGE SYSTEM

ASME 2014 International Mechanical Engineering Congress & Exposition (IMECE14)

Ali Siahpush, James O'Brien, John Crepeau, Piyush Sabharwall

July 2015

ASME 2014 International Mechanical Engineering Congress & Exposition
IMECE14
November 14–20, 2014, Montreal, Canada

IMECE2014-39786

SCALE ANALYSIS AND EXPERIMENTAL RESULTS OF A SOLID/LIQUID PHASE-CHANGE THERMAL ENERGY STORAGE SYSTEM

Ali Siahpush
Ferris State University
Big Rapids, MI, USA

James O'Brien
Idaho National Laboratory
Idaho Falls, Idaho, USA

John Crepeau
University of ID
Moscow, ID, USA

Piyush Sabharwall
Idaho National Laboratory
Idaho Falls, Idaho, USA

ABSTRACT

A detailed experimental study has been carried out to evaluate the heat transfer performance of a solid/liquid phase-change thermal energy storage system. The phase-change material (PCM) and metal foam are contained in a vertically oriented test cylinder that is cooled or heated at its outside boundary, resulting in radially inward melting, respectively. Detailed quantitative time-dependent volumetric temperature distributions and melt-front motion and shape data were obtained. As the PCM melts, the interface moves away from the surface of the heat source/sink, and a thermal resistance layer is built up, resulting in a reduced heat transfer rate and/or increased temperature difference between the system to be cooled (or heated) and the PCM. The phase-change medium was 99% pure eicosane, with a melting temperature of 36.5°C. Results have been generalized to apply to any low-Stefan number PCM.

A heat transfer scale analysis was used in order to help in interpretation of the data and development of heat transfer correlations. In the scale analysis, conduction heat transfer in the solid and natural convection heat transfer in liquid were considered. Comparison of experimental data with scale-analysis predictions of the solid-liquid interface position and temperature distribution was performed.

INTRODUCTION

Phase change thermal storage and thermal control devices have been discussed extensively in the literature. These articles often refer to a device, which is used to either thermally control a component or store energy by utilizing a material, which undergoes a change of phase (PCM) in the temperature range of interest for the process.

Interest in the heat transfer aspects of freezing and melting has been increased in recent years by the proposed use of phase-change processes for the storage of thermal energy. A survey of the experimental literature [1] reveals a strong concentration of effort on melting or freezing outside of heated or cooled cylinders embedded either vertically or horizontally in a phase-change medium.

The solution of moving-boundary problems with phase change has been of special interest due to the inherent difficulties associated with the nonlinearity of the interface conditions and the unknown locations of the moving boundaries. Exact closed-form solutions of phase-change problems are available only for a limited number of cases such as the Stefan problem. A variety of approximate analytical solution techniques have been developed, including the heat balance integral [2], variational [3], embedding [4], and perturbation techniques [5, 6]. In addition, efforts to solve phase-change problems numerically have produced such diverse solution methods as the enthalpy [7, 8], apparent heat capacity [9], isotherm migration [10], and coordinate transportation methods [11–16]; these methods have been introduced by researchers mainly to overcome the difficulties in handling moving boundaries.

Lunardini [17] and Pouhkakus [18] investigated melting and freezing of a phase-change medium contained in a vertical cylinder. They studied outward phase change in detail for many cases including freezing of a subcooled liquid, zero subcooled, and melting of a superheated, and zero superheat in infinite domain and finite geometry. Lunardini has also performed limited study on inward melting and freezing of a phase-change medium contained in a vertical cylinder.

Fundamental heat transfer experiments were performed for freezing of an initially superheated or nonsuperheated liquid in a cooled vertical cylindrical container (inward freezing) by Sparrow [19]. He concluded that, although the latent energy is the contributor to the total extracted energy, the total sensible energies could make a significant contribution, especially at large tube wall subcooling, large liquid superheating, and short freezing time. Natural convection effects in the superheated liquid were modest and were confined to short freezing times.

The primary objective of this work is to evaluate inward melting of a solid/liquid phase change system in a cylindrical enclosure. In the melting experiments, the phase change medium used was 99% pure n-eicosane paraffin, with a melting temperature of 36.5ºC.

EXPERIMENTAL SETUP AND PROCEDURE

The experiments were performed in a copper test vessel. In order to provide a controlled, constant wall temperature thermal boundary condition, a pair of copper tubes was wrapped and soldered around the outside of the copper test vessel, with two tube inlets, each at opposite ends of the test vessel. In this manner, the double-wrapped tubing acted like a counter flow heat exchanger to provide a uniform wall temperature boundary condition around the outer periphery of the test vessel. The test vessel was fabricated from a large copper tube with an inside diameter of 15.55 cm, an outside diameter of 16.19 cm, and a height of 30.48 cm.

Lids made of acrylic plastic sealed the test vessel on the top and bottom. The thermal conductivity of acrylic is much lower than the thermal conductivity of the PCM and the copper test vessel, which helped reduce the end effects. Two small vertical copper tubes were placed in the top cap to enable removal of excess PCM during melting and to prevent overflowing, as well as to provide a passage of the thermocouple wires. The test vessel system was insulated using 10-cm-thick fiberglass fitted around the entire vessel and caps. A constant temperature bath was selected to supply cooling/heating fluid to the copper heat exchange tubes that kept the outer wall of the container at constant temperature.

For these experiments, 99% pure eicosane ($C_{20}H_{42}$) was chosen as the PCM. Eicosane was desirable because it has a single fusion temperature (36.5°C), which is just slightly higher than ambient temperature, making it convenient for phase change experimentation. Low-temperature heating can be used to melt the PCM and ambient-temperature cooling can be used to refreeze it. In addition, the proximity of the melting point to ambient temperature results in reduced heat losses to the environment. The thermo-physical properties of eicosane are reasonably well established, and the thermal conductivity of the solid eicosane is given as 0.423 W/mK [20].

For the series of tests, a plastic tree was fabricated to hold the thermocouples (TCs) in place. Four additional TCs deployed along the outside height of the copper test vessel measured the wall temperature. Numerous melting tests were performed at various wall temperatures. At the termination of the tests, all of the TCs indicated that the entire eicosane volume was in thermal equilibrium with the constant temperature water bath.

EXPERIMENTAL RESULTS FOR MELTING EICOSANE

For the experiment to be detailed in this section, the eicosane phase-change material had an initial temperature of 10°C and a final temperature of 50ºC.

In the presence of natural convection in the melt region, it is convenient to identify first four regimes, I–IV, whose main characteristics are sketched schematically in Figure 1 [21]. In this figure, the dashed line represents the phase-change interface front. On the right of the dashed line is the liquid region and on its left, the solid region. The “Conduction Regime” (I) is dominated by pure thermal diffusion. The “Transition Regime” (II) occurs when a natural convection flow carves its own convection-dominated zone in the upper part of the liquid region, while the lower part remains ruled by conduction. The “Quasi-Steady Natural Convection Regime” (III) begins when the convection-dominated zone of the preceding regime fills the entire height of the cylinder. Finally, the arrival of the liquid-solid interface at the centerline marks the beginning of the “Variable Height Regime” (IV).

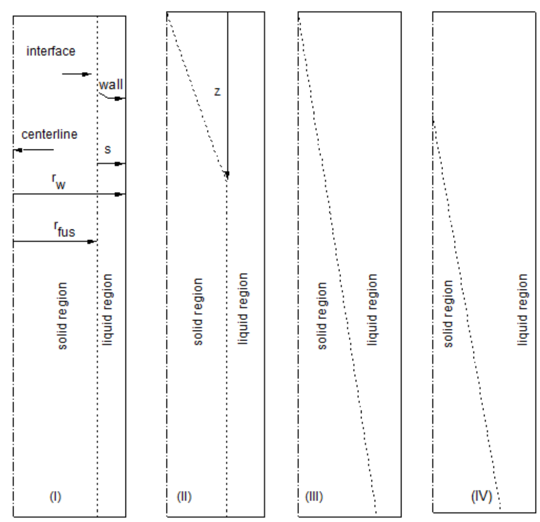

Figure 1. Four regimes of melt.

Heat Transfer and Scaling Analysis

The object of scale analysis is to use the basic principles of convection heat transfer in order to produce order-of-magnitude estimates for quantities of interest (in our case Nusselt number and radius of fusion). In order for the results of the scale analysis (a functional proportionality) to be converted into an equality, a proportionality constant must be inserted into the equations describing the radius of fusion and the Nusselt number. These constants varied between 0.1 and 10 (± an order of magnitude) and they are different for each case.

Conduction Regime (I)

If we can assume that components and the solid PCM are at the fusion temperature, then immediately after t=0, the melting process is governed by pure conduction heat transfer. The heat flux across the very thin liquid film is absorbed by the latent heat of fusion at the liquid-solid interface. Referring to Figure 2, this heat balance, in cylindrical coordinates, can be expressed as

$$2\pi r_{fus} k_l H \frac{T_w - T_{fus}}{r_w - r_{fus}} \approx \Delta h_{fus} \frac{dm}{dt} \tag{1}$$

where H is the height of the tank, and dm/dt is the mass rate of melting. The last term on the right of Equation (1) may be expressed as

$$\frac{dm}{dt} = \frac{d}{dt}(\rho_{liq}\pi(r_w{}^2 - r_{fus}^2)H) \tag{2}$$

Substituting Equation (2) into (1), and integrating yields the following solution for the radius of fusion in the conduction regime.

$$s = r_w - r_{fus} \approx H\theta^{1/2}$$

or

$$r_{fus} \approx r_w - H\theta^{1/2} \tag{3}$$

where s is defined as the thickness of the liquid PCM (m) in a radial direction, and θ is a dimensionless time defined as

$$\theta = \frac{k_l (T_w - T_{fus})}{\rho_l \Delta h_{fus} H^2} t = St_l.Fo \tag{4}$$

Where St_l is the liquid Stefan number. The liquid Stefan number is defined as

$$Ste_l = \frac{c_{pl}(T_w - T_{fus})}{\Delta h_{fus}} \tag{5}$$

For comparison to heat transfer results obtained at later times, it is desirable to express the results of the pure-conduction Regime (I) in terms of a convection heat transfer coefficient and Nusselt number. The Nusselt number (Nu_H) based on cylinder height is defined as [23]

$$Nu_H = \frac{hH}{k_l} \tag{6}$$

where h is the convection heat transfer coefficient. Heat transfer at the melt interface can be expressed in terms of a heat transfer coefficient using

$$2\pi r_{fus} Hh(T_w - T_{fus}) \approx 2\pi r_{fus} Hk_l \frac{(T_w - T_{fus})}{s} \tag{7}$$

From equation (7), we can conclude that the convection heat transfer coefficient for Regime (I) can be expressed as

$$h \approx \frac{k_l}{s} \tag{8}$$

Substituting Equation (8) into Equation (6) yields the Nusselt number (Nu_I) that corresponds to the pure conduction regime.

$$Nu_I \approx \frac{H}{s} \tag{9}$$

Substituting equation (3) into From Equation (9) yields

$$Nu_I \approx \frac{H}{s} = \frac{H}{H\theta^{1/2}} = \theta^{-1/2} \tag{10}$$

Transition/Mixed Regime (II)

For the analysis of this regime, we will assume the height of the upper convection region is z, and the remainder of the liquid height (H – z) continues to be controlled by conduction.

In the upper zone, the thermal boundary layer thickness (δ_z) is smaller than the horizontal dimension of the carved-out upper zone. It should be noted that, at the location where δ_z is of the same order as the gap thickness of the lower conduction zone, convection becomes negligible.

$$\delta_z = s \tag{11}$$

In the steady-state condition, the heat conducted from the wall is carried upward by convection inside the thermal boundary layer. In that thermal boundary layer region where r ≈ δ and z ≈ H, consider the conservation of mass, z-momentum, and energy. Then scales of mass, z momentum, and energy equations become

$$\frac{u}{\delta}, \frac{u}{\delta}, \approx \frac{w}{H}$$

$$u\frac{w}{\delta}, \frac{w^2}{H} \approx g\beta\Delta T, \nu(\frac{1}{\delta}\frac{w}{\delta}, \frac{w}{\delta^2}, \frac{w}{H^2}) \tag{12}$$

$$u\frac{\Delta T}{\delta}, w\frac{\Delta T}{H} \approx \alpha(\frac{\Delta T}{\delta^2}, \frac{\Delta T}{\delta^2}, \frac{\Delta T}{H^2})$$

where $\Delta T = T_w - T_{fus}$ is the scale of T-T_{fus}. Since $\delta << H$, the two terms w/H^2, and $\Delta T/H^2$ are much smaller than w/δ^2, and $\Delta T/\delta^2$, respectively, and may be ignored.

From the continuity equation, we may conclude that

$$\frac{u}{\delta} \approx \frac{w}{H} \tag{13}$$

Substitution of the continuity equation into the energy equation yields

$$\frac{w}{H} \approx \frac{\alpha}{\delta^2} \tag{14}$$

Also substitution of the continuity equation into the scale of the z-momentum of Equation (12) yields

$$\frac{w^2}{H} \approx \beta g \Delta T,\ \nu \frac{w}{\delta^2} \tag{15}$$

Dividing both sides of Equation (15) by the buoyancy scale ($\beta g \Delta T$) and using Equation (14) to eliminate the vertical velocity scale (w), we obtain

$$(\frac{H}{\delta})^4 Ra_H^{-1} Pr^{-1} \approx (\frac{H}{\delta})^4 Ra_H^{-1}, 1 \tag{16}$$

where Ra_H, and Pr are the Rayleigh, and Prandtl numbers, respectively, defined as

$$Ra_H = \frac{\beta g \Delta T H^3}{\alpha \nu}$$
$$Pr = \frac{\nu}{\alpha} \tag{17}$$

where ν is the kinematic viscosity (m/sec^2). In our case where the Pr is much greater than one (Pr>>1), the term on the left of Equation (16) is much smaller than the first term on the right, so it can be ignored. Then, Equation (16) will result in an expression for thermal boundary layer thickness as

$$\delta \approx H Ra_H^{-1/4} \tag{18}$$

For the upper convection region (height of z), Equation (6.26) can be used to show the convection thermal boundary layer thickness (δ_z).

$$\delta_z \approx z Ra_z^{-1/4} \tag{19}$$

where Ra_z is the Rayleigh number based on the height, z, and is expressed as

$$Ra_z = (\frac{z}{H})^3 Ra_H \tag{20}$$

Combination of Equations (3), (11), (19), and (20) gives an expression for z.

$$z \approx H Ra_H \theta^2 \approx s Ra_H \theta^{3/2} \tag{21}$$

Equation (21) suggests that the transition regime ends, when $z \approx H$, at a time of order (θ_{II})

$$\theta_{II} \approx Ra_H^{-1/2} \tag{22}$$

The total heat transfer rate through the heated wall, q_{II} (w), has two components. The first component is convection over the z height, and the second is conduction over the remainder of the height (H – z).

$$q_{II} \approx 2\pi r_w [k_l z \frac{T_w - T_{fus}}{\delta_z} + k_l (H - z) \frac{T_w - T_{fus}}{s}] \tag{23}$$

Substituting the q_{II} definition, Equation (23), into the Nusselt number expression $(Nu_H = q_{II} / [2\pi r_w (T_w - T_{fus}) k_l]$, and utilizing Equations (3), (19), and (21), will result in the transition Nusselt number (Nu_{II}).

$$Nu_{II} \approx \theta^{-1/2} + Ra_H \theta^{3/2} \tag{24}$$

The Regime (II) Nusselt number is made up of two components, one due to conduction, the first term on the right of Equation (24), and the other due to convection, the last term on the right of Equation (24). The heat transfer scaling law, Equation (24), holds at $\theta = 0$ until the convection height (z) extends all the way to the bottom of the tank ($z \approx H$).

The Quasi-steady Convection Regime (III)

At nondimensional times greater than $\theta_{II,}$ the quasi-steady convection zone fills the entire liquid space of height H. As we discussed earlier, at the end of the Regime (II), which is the beginning of Regime (III), from Equation (24) the Nusselt number scale ($Nu_{min\text{-}III}$) is

$$Nu_{min\text{-}III} \approx Ra_H \theta_{II}^{3/2} \tag{25}$$

Substitution of θ_{II} from Equation (22) into Equation (25) yields

$$Nu_{min\text{-}III} \approx Ra_H^{1/4} \tag{26}$$

This Nusselt number scale is the minimum value for Regime (III). The Nusselt number in Regime (III) is time-dependent but does not change significantly with respect to time. Since in the convection regime, the melt front is always deformed, it is more appropriate and convenient to present the front location based on a height-averaged melt-front location.

At the interface, the convection heat transfer rate (q_{conv}) balances the latent heat rate (q_{fus}) released from the interface. The left side of Equation (7) expresses a relation for the convection heat transfer rate. Substitution of Equations (6) and (26) into Equation (7) results in the scale of convection heat transfer rate (q_{conv}).

$$q_{conv} \approx \frac{k_l}{H} Ra_H^{1/4} (H \times 1)(T_w - T_{fus}) \tag{27}$$

where (H x 1) is the unit area perpendicular to the heat transfer direction. Substitution of Equation (2) into Equation (1) gives q_{fus} as

$$q_{fus} = \pi H \rho_l \Delta h_{fus} (-2 r_{fus}) \frac{dr_{fus}}{dt} \tag{28}$$

Equating and then integrating Equations (27) and (28) results in an equation that describes the position of the interface with respect to the dimensionless time.

$$r_{fus} \approx \sqrt{r_w^2 - \frac{k_l Ra_H^{1/4} (T_w - T_{fus})}{\rho H \pi \Delta h_{fus}} t} = \sqrt{r_w^2 - \frac{1 \times H}{\pi} Ra_H^{1/4} \theta} \tag{29}$$

Equations (26) and (29) hold until the average solid-liquid interface reaches the centerline. At $r_{fus} = 0$, the convection regime expires and the dimensionless time (θ_{III}) will be

$$\theta_{III} \approx \frac{\pi r_w^2}{1 \times H} Ra_H^{-1/4} \tag{30}$$

The Variable Height Regime (IV)

We now turn our attention to the last regime, in which the remaining solid shrunk as its uppermost point, at height of H, descended along the centerline. Liquid circulation continues, as in the convection regime, however, the heat transfer and melting rates depend on the size of the remaining solid.

Bejan [22, 23], in order to determine the scales of this regime, made assumptions concerning the shape of the solid region. He assumed that early enough in Regime (IV), the fusion radius is fixed and the height of the frozen/solid eicosane (h_{IV}) decreases. Then, in the intermediate stage of Regime (IV), the liquid-solid interface advanced such that both r_{fus} and h_{IV} decreased at the same rate (the interface advanced while remained parallel to itself). Finally, when the solid disappeared almost totally ($h_{IV} << H$) leaving nearly horizontal zone ($h_{IV} << r_{fus}$).

To begin the analysis, the first stage of the Regime (IV) is explored to define the scale of the Nusselt number. The scale of the Nusselt number in this stage is the order of $Ra_{h_{IV}}^{1/4}$ (Rayleigh number based on h_{IV}) since the interface resistance controlled the heat transfer rate that melted the solid. The Rayleigh number based on h_{IV} is related to the Rayleigh number based on the total height such that

$$Ra_{h_{IV}} \approx \left(\frac{h_{IV}}{H}\right)^3 Ra_H \tag{31}$$

An energy balance at the solid-liquid moving interface requires that

$$\left(\frac{h_{IV}}{H}\right)^{3/4} Ra_H^{1/4} k_l \; x \, 1 (T_w - T_{fus}) \approx \Delta h_{fus} \frac{dm}{dt} \tag{32}$$

where dm/dt is defined from Equation (2) as

$$\frac{dm}{dt} = \frac{d}{dt}(\rho_{liq} \pi (r_w^{\ 2} - r_{fus}^2) h_{IV}) = (\rho_{liq} \pi (r_w^{\ 2} - r_{fus}^2) \frac{dh_{IV}}{dt} \tag{33}$$

From Equation (4), dt can be expressed as a function of dθ.

$$dt = \frac{\rho_l H^2 \Delta h_{fus}}{k_l (T_w - T_{fus})} d\theta \tag{34}$$

Substitute Equation (34) into (33) and then into (32) results in the energy balance at the interface.

$$\int_{\theta_{III}}^{\theta} \frac{Ra_H^{1/4} H^{5/4} x \, 1}{\pi (r_w^2 - r_{fus}^2)} d\theta \approx -\int_H^{h_{IV}} h_{IV}^{\ -3/4} dh_{IV} \tag{35}$$

Integration of Equation (35) gives the rate of Regime (IV) height decrease as

$$\left(\frac{h_{IV}}{H}\right)^{1/4} \approx 1 - \frac{1}{4} \frac{Ra_H^{1/4} H \times 1}{\pi (r_w^2 - r_{fus}^2)} (\theta - \theta_{III}) \tag{36}$$

It should be noted that this equation is valid when $\theta > \theta_{III}$. This regime ends (the solid will disappear entirely) at a time θ_{IV} when $h_{IV} << H$, which, according to Equation (36), is

$$\theta_{IV} - \theta_{III} \approx 4 \frac{\pi (r_w^2 - r_{fus}^2)}{H \times 1} Ra_H^{-1/4} \tag{37}$$

If Equation (36) is substituted into (31), the result is the scale of the Nusselt number for Regime (IV).

$$Nu_{IV\text{-}1} \approx Ra_H^{1/4} \left[1 - \frac{1}{4} \frac{Ra_H^{1/4} H \times 1}{\pi (r_w^2 - r_{fus}^2)} (\theta - \theta_{III})\right]^3 \tag{38}$$

In the intermediate stage of the last regime, the liquid-solid interface advances such that h_{IV} and r_{fus} decrease at the same rate. The energy balance at the interface, Equation (32), still can be applied in this case, however, $dr_{fus}/dt \approx dh_{IV}/dt$. This equation can be solved for fusion radius of Regime (IV). The result is

$$r_{fus}^{5/4} \approx r_w^{5/4} - \frac{5}{8}\frac{H^{5/4}}{\pi} Ra_H^{1/4}(\theta - \theta_{III}) \quad (39)$$

The scale of the interface location from Equation (39) is compared with the average fusion radius evaluated from data in Figure 3. This figure shows that the scale of the average fusion radius matches the prediction for a portion of Regime (III) exactly. The r_{fus}/r_w ratio decreases almost linearly, which is confirmed also by the shape of the data in this figure. This scale matches the data all the way to the end of experiment ($Nu \approx 0$) and it is valid to assume that there is no need to explore the last stage of the Regime (IV) to express the scale of the fusion radius.

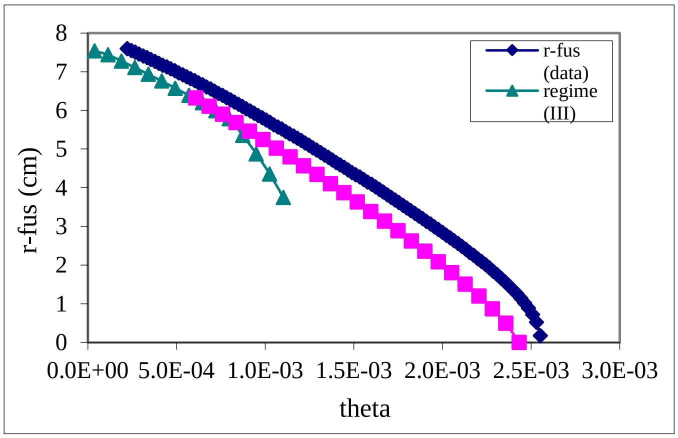

Figure 3. Regime III and IV average fusion radius vs. data.

As mentioned earlier, the scale of the Nusselt number in this regime is the order of $Ra_{h_{IV}}^{1/4}$. Utilizing Equation (31), the scale of the Nusselt number, Nu_{IV-2} can be expressed as

$$Nu_{IV\text{-}2} \approx (Ra_{h_{Iw}})^{1/4} \approx (\frac{r_{fus}}{r_w})^{3/4} Ra_H^{1/4} \quad (40)$$

Note that the h_{IV}/H is replaced by r_{fus}/r_w, since we assumed $dr_{fus}/dt \approx dh_{IV}/dt$. Equation (39) expresses the ratio of the fusion radius to the fusion radius at the end of Regime (III). Substitution of Equation (39) into Equation (40) yields the Nusselt number of the intermediate stage of the Regime (IV).

$$Nu_{IV\text{-}2} \approx \frac{Ra_H^{1/4}}{r_w^{3/4}}[r_w^{5/4} - \frac{5}{8}\frac{H^{5/4}}{\pi} Ra_H^{1/4}(\theta - \theta_{III})]^{3/5} \quad (41)$$

Based on the scale analysis of all four regimes, it is clear that Regimes (I) and (II) occupy relatively a short period of time and they disappear quickly into Regime (III). These two regimes do not contribute significantly to the scale of the fusion radius and may easily be ignored. On the other hand, the Nusselt number of Regimes (I) and (II) cannot be disregarded. The Nusselt numbers of the Regimes (I) and (II) started at infinity at the beginning of the experiment. As time progressed, the Nusselt numbers decreased proportional to the dimensionless time ($\theta^{1/2}$). As conduction gradually disappeared, convection appeared and its effect eventually dominated the heat transfer. In Regime (III), the Nusselt number is quasi-steady. When the Regime (IV) started, in the stage one of Regime (IV), the Nusselt number rapidly decreased as a function of $[1-(\theta-\theta_{III})]^3$, but toward the very end of the experiment, intermediate stage of Regime (IV), the Nusselt number changes as a function of $[1-(\theta-\theta_{III})]^{3/5}$. The complete history of the scale of the Nusselt numbers of all four regimes is shown in Figure 4.

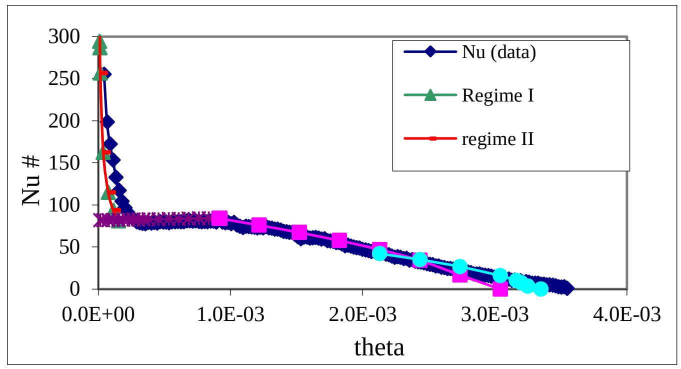

Figure 4. Complete history of the heat transfer scale.

UNCERTAINTY ANALYSIS

An estimate of the uncertainty in the calculated result (δR), based on a constant-odds formulation, is given by [24]

$$\frac{\delta R}{R} = \frac{1}{R}[(\frac{\partial R}{\partial X_1}\delta X_1)^2 + (\frac{\partial R}{\partial X_2}\delta X_2)^2 + \ldots + (\frac{\partial R}{\partial X_J}\delta X_J)^2]^{1/2} \quad (42)$$

where $\partial R/\partial X_J$ is the partial derivative of R with respect to X_J, and δX_J is the uncertainty of X_J. In many engineering cases, R can be expressed as a product string. In such cases, R is expressed as

$$R = x_1^a x_2^b \ldots\ldots\ldots \quad (43)$$

In this case, the relative uncertainty of R is expressed as [25, 26]

$$\frac{\delta R}{R} = [(a\frac{\delta x_1}{x_1})^2 + (b\frac{\delta x_2}{x_2})^2 + \ldots\ldots]^{1/2} \quad (44)$$

Utilizing Equation (42), the uncertainty in the radius of fusion for melting can be expressed as

$$\frac{\delta r_{fus}}{r_{fus}} = \frac{1}{r_{fus}}[(\frac{\partial r_{fus}}{\partial Q_1}\delta Q_1)^2 + (\frac{\partial r_{fus}}{\partial Q_2}\delta Q_2)^2]^{1/2} \quad (45)$$

Where Q_1 is the incremental heat transfer to the system, and Q_2 is the total heat transfer to each component. Utilizing Equation (44), the uncertainties of Q_1 and Q_2 are defined as

$$\delta Q_1 = Q_1 \left[\left(\frac{\delta \dot{m}}{\dot{m}}\right)^2 + \left(\frac{\delta \Delta T_{meter}}{\Delta T_{meter}}\right)^2\right]^{1/2}$$

(46)

$$\delta Q_2 = Q_2 \left[\left(\frac{\delta \Delta T_{TC}}{\Delta T_{TC}}\right)^2\right]^{1/2} = Q_2 \frac{\delta \Delta T_{TC}}{\Delta T_{TC}}$$

where $\delta \dot{m}/\dot{m}$ is the relative uncertainty for the mass flow rate of water, $\delta \Delta T_{meter}/\Delta T_{meter}$ is the uncertainty of the temperature difference between inlet and outlet of the water flow, and $\delta \Delta T_{TC}/\Delta T_{TC}$ is the uncertainty of the temperature differences measured with thermocouples. The ΔT_{TC} was measured by thermocouples (0.005-inch-diameter, OMEGA TT-K-36, type-K thermocouple). In estimating the relative uncertainty, $\delta \Delta T_{TC}/\Delta T_{TC}$, thermocouple manufacturer and the data acquisition/control (HP model 3852A) specifications were taken into account. These estimates indicated that the thermocouple uncertainty is temperature dependent.

Results of Equation (45), for melting are presented in Figure 5. This figure presents the uncertainty of the radius of fusion with respect to time. In this figure, as expected at t=0, the uncertainty with respect to the radius of fusion is zero (at the wall radius) and as time progressed, the uncertainty of radius of fusion increased due to increase in uncertainties of the cumulative heat transfer (Q_1 and Q_2) and the fact that, as the test progresses, r_{fus} decreases, approaching zero for large times.

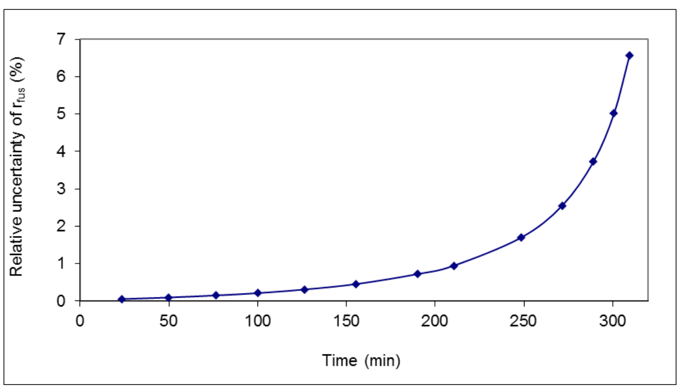

Figure 5. Radius of fusion uncertainty (melting).

The only experimental uncertainty associated with the measured Nusselt number is the uncertainty of the instantaneous heat transfer to the eicosane (q_3). The relative Nusselt number uncertainty ($\delta Nu/Nu$) can then be expressed as

$$\frac{\delta Nu}{Nu} = \frac{1}{Nu}\left[\left(\frac{\partial Nu}{\partial q_3}\delta q_3\right)^2\right]^{1/2} = \frac{1}{Nu}\left(\frac{\partial Nu}{\partial q_3}\delta q_3\right) \qquad (47)$$

where $\partial Nu/\partial q_3$ is the partial derivative of Nu with respect to q_3, and δq_3 is the uncertainty of q_3. Note that the same equation (Equation 46) predicting δQ_2 may be utilized to predict δq_3 (Q_2 replaced by q_3).

Utilizing Equation (47) indicates that the relative uncertainty of the Nusselt numbers were independent of time (in the worst case approximately 4%) and a typical values of them are: Nu=5.6%.

CONCLUSION

A detailed experimental study has been carried out to evaluate the heat transfer performance of a solid/liquid phase-change thermal energy storage system. The phase-change material is contained in a vertically oriented test cylinder that is heated at its outside boundary (inward interface motion). The PCM employed in this work was 99% pure eicosane paraffin having a melting point of 36.5°C. Based on this work, the following conclusions/observations related to melting were obtained:

1. Initial subcooling of the solid decreased the rate of melting and, correspondingly, the rate of sensible heat storage in the liquid.

2. The melting problem is characterized by a conduction heat transfer regime (“Conduction Regime”) at early times followed by a transition (“Transition/Mixed Convection and Conduction Regime”) to a natural convection dominated regime (“Quasi-Steady Natural Convection Regime”). Finally, the arrival of the liquid-solid interface at the centerline marks the beginning of the “Variable Height Regime”. From this time, the height of the liquid-solid interface decreases steadily until the solid region disappears entirely.

3. An examination of the experimentally observed pattern of melting confirmed the progression through the four regimes of melting. For very short melting times, vertical near-wall isotherms indicated that conduction was the sole means of heat transfer. However, the upward flow of fluid, due to the natural convection which accompanied melting, caused the solid material to take on a curvature near its top. The accumulation of liquid atop the solid caused a downward melting in addition to inward melting. This type of melting was perpetuated by natural convection, which developed in the liquid region. Melt shapes corresponding to the completion of selected tests were measured and are reported. The inverted bell shape of the cavities demonstrated the dominant role of natural convection in the melting problem.

The model presented here to predict melting was based on a scale analysis which considers conduction and convection heat transfer with zero superheat contained in the liquid eicosane. Predictions obtained from model results have been compared to the experimentally measured radius of fusion values, evaluated utilizing a volume-averaged technique. The results were within 10% of the data measurements in the worst case.

REFERENCES

[1] R. Viskanta, A. G. Bathelt, and N. W. Hale, "Latent Heat-of-Fusion Energy Storage: Experiments on Heat Transfer During Solid-Liquid Phase Change," Proceedings, Third Miami Conference on Alternative Energy Sources, December 1980.

[2] T. R. Goodman, "Heat Balance Integral-Further Considerations and Refinements," J. Heat transfer, 83, 83–86, 1991.

[3] M. A. Biot and H. Daughaday, "Variation Analysis of Ablation," J. Aerospace Science, 29, 227–229, 1962.

[4] B. A. Boley and H. P. Yagoda, "The Starting Solutions for Two-Dimensional Heat Conduction Problems with Phase Change," Q. Applied Mathematics, 27, 223–246, 1969.

[5] R. I. Pedroso and G. A. Domoto, "Perturbation Solutions for Spherical Solidification of Saturated Liquid," J. Heat Transfer, 95, 42–46, 1973.

[6] R. I. Pedroso and G. A. Domoto, "Exact Solution by Perturbation Method for Planer Solidification of a Saturated Liquid with Convection at the Wall," Int. J. Heat Mass Transfer, 16, 1816–1819, 1973.

[7] N. Shamsundar and E. M. Sparrow, "Effect of Density Change on Multidimensional Conduction Phase Change," J. Heat Transfer, 97, 550–557, 1976.

[8] A. B. Crowley, "Numerical Solution of Stefan Problems," Int. J. Heat Mass Transfer, 21, 215–219, 1978.

[9] C. Bonacina, G. Comini, A. Fasano, and M. Primicerio, "Numerical Solution of Phase-Change Problem," Int. J. Heat Mass Transfer, 16, 1825–1832, 1973.

[10] J. Crank and R. S. Gupta, "Isotherm Migration Method in Two Dimensions," Int. J. Heat Mass Transfer," 18, 1101–1117, 1975.

[11] E. M. Sparrow and W. Chuck, "An Implicit/Explicit Numerical Solution Scheme for Two Phase-Change Problem," Numerical Heat Transfer, 7, 1–15, 1984.

[12] M. E. Sparrow, S. Ramadhyani, and S. V. Patankar, "Effect of Subcooling on Cylindrical Melting," J. Heat Transfer, 100, 395–402, 1978.

[13] F. B. Cheung, T. C. Chawla, and D. R. Pedersen, "The Effect of Heat Generation and Wall Interaction on Freezing and Melting in a Finite Slab," Int. J. Heat Mass Transfer, 27, 29–37, 1984.

[14] T. Saitoh, "Numerical Method for Multi-Dimensional Freezing Problems in Arbitrary Domains," J. Heat Transfer, 100, 294–299, 1978.

[15] J. L. Duda and M. F. Malone, "Analysis of Two-Dimensional Diffusion-Controlled Moving Boundary Problems," Int. J. Heat Mass Transfer, 18, 901–910, 1956.

[16] C. F. Hsu, E. M. Sparrow, and S. V. Patankar, "Numerical Solution of Moving Boundary Problems by Boundary Immobilization and a Control-Volume-Based Finite Difference Scheme," Int. J. Heat Mass Transfer, 24, 1335–1343, 1981.

[17] V. J. Lunardini, *Heat Transfer with Freezing and Thawing*, Elsevier Science Publication, New York, 1991.

[18] D. Poulikakus, *Conduction Heat Transfer*, Perntice Hall, New Jersey, 1994.

[19] E. M. Sparrow and J. A. Broadbent, "Freezing in a vertical Tube," Journal of Heat Transfer, Vol. 105, pp. 217–225, May 1983.

[20] D. V. Hale, M. J. Hoover, and M. J. O'Neill, "Phase Change Handbook," NASA Contractor Report, NASA-CR-61363, September 1971.

[21] P. Jany and A. Bejan, "Scale of Melting in the Presence of Natural Convection in a Rectangular Cavity Filled with Porous Medium," Transactions of the ASME, Vol. 110, pp. 526–528, May 1988.

[22] A. Bejan, *Convection Heat Transfer*, Second Edition, John Wiley & Sons, Inc., New York, 1995.

[23] P. Jang and A. Bejan, "Scaling Theory of Melting with Natural Convection in an Enclosure," Int. J. Heat Mass Transfer, Vol. 31. No. 6, pp. 1221–1235, 1988.

[24] H. W. Coleman and W. G. Steele, *Experimentation and Uncertainty Analysis for Engineers*, John Wiley and Sons, New York, New York, 1989.

[25] R. J. Moffat, "Contributions to the Theory of Single-Sample Uncertainty Analysis," Journal of Fluids Engineering, Vol. 104, pp. 250–259, June 1982.

[26] R. J. Moffatt, "Describing the Uncertainties in Experimental Results," Experimental Thermal and Fluid Science, Vol. 1, pp. 3–17, 1988.